Benthic biolayer structure controls whole-stream reactive transport

Kevin R. Roche[1,2], **Marco Dentz** [1]

[1]Spanish National Research Council (IDAEA-CSIC), Barcelona, Spain
[2]Department of Civil Engineering, Boise State University
[1]c/ Jordi Girona, 18, 08034 Barcelona, Spain
[2]1910 University Dr, Boise, ID 83725, USA

Key Points:

- Storage in non-reactive sublayer causes long contaminant survival times
- Reach-scale reaction kinetics cannot be captured by constant rate model
- Upscaled model quantifies all aspects of reaction and mass transfer

Corresponding author: Kevin R. Roche, `kevinrroche@boisestate.edu`

Abstract

Hyporheic zone reaction rates are highest just below the sediment-water interface, in a shallow region called the benthic biolayer. Vertical variability of hyporheic reaction rates leads to unexpected reaction kinetics for stream-borne solutes, compared to classical model predictions. We show that deeper, low-reactivity locations within the hyporheic zone retain solutes for extended periods, which delays reactions and causes solutes to persist at higher concentrations in the stream reach than would be predicted by classical approaches. These behaviors are captured by an upscaled model that reveals the fundamental physical and chemical processes in the hyporheic zone. We show how time scales of transport and reaction within the biolayer control solute retention and transformation at the stream scale, and we demonstrate that accurate assessment of stream-scale reactivity requires methods that integrate over all travel times.

Plain Language Summary

Dissolved materials such as carbon, nutrients, and contaminants react as they move through the river network. Some locations in the river are far more reactive than others, and it is challenging to predict how this spatial variability of reaction rates controls the reactivity of the entire stream. One hotspot of high reactivity is the benthic biolayer, a thin region below the sediment-water interface with an abundance of microbial activity, and below which reactivity decreases to very low values. We use a mathematical model to quantify the benthic biolayer's contribution to whole river material transformation, based on the biolayer's thickness and reactivity. We show that thin or less reactive biolayers allow dissolved mass to become sequestered for long periods deep in the streambed, leading to low but persistent concentrations long after the mass is introduced to the river. These theoretical advances improve our understanding of how measurable features of the river – namely, the depth-dependent reaction rates within the streambed – are directly related to biogeochemical transformations and contaminant retention timescales in rivers.

1 Introduction

A defining feature of rivers is the transition in physical and chemical characteristics across the sediment-water interface (SWI). Downstream velocities, mixing rates, and light availability decrease rapidly at the SWI to viscous flows and light limited conditions (Jones & Mulholland, 1999). This transition zone, called the benthic biolayer, contributes disproportionately to the biologically-mediated transformation of reactive solutes and fine particulate matter in the river corridor, including heterotrophic carbon respiration, nutrient cycling, and trace contaminant degradation (Battin et al., 2008; Kunkel & Radke, 2008; Marzadri et al., 2017). Fluvial ecosystems are highly sensitive to physical perturbations and elevated contaminant concentrations in the biolayer, since this region supplies refugia and energy (as microbial biomass) for freshwater vertebrates (Jones & Mulholland, 1999; Cardenas et al., 2016; Moran et al., 2017). Structural features of the biolayer, such as its depth and reactivity, are therefore important predictors of whole-river reactivity and ecosystem health.

Dissolved oxygen depletes as aerated surface water propagates deeper into the hyporheic zone (HZ), leading to conditions that sustain microbial communities with higher tolerance for anoxia and slower metabolism. The stratification of chemical conditions and microbial biomass below the sediment-water interface (SWI) creates sharp gradients in reaction rates, as well as regions of low reactivity below the biolayer (Kunkel & Radke, 2008; Harvey et al., 2013; Knapp et al., 2017). The vertical profile of reaction rates is challenging to determine not only because steep concentration gradients are difficult to measure in pore waters, but also because various transport processes are simultaneously active (e.g., advective pumping, molecular and turbulent diffusion, mechanical dispersion). These processes are often grouped using scaling laws to estimate vertical solute

fluxes across the SWI. Scaling predictions are related to subsurface concentrations by assuming that solutes diffuse vertically (O'Connor & Harvey, 2008; Grant et al., 2012), which allows the reaction profile to be inferred from a diffusion-reaction or similar 1-D transport model (Harvey et al., 2013; Knapp et al., 2017; Schaper et al., 2019).

Recent modeling efforts strongly suggest that spatial variability of reaction rates in the biolayer controls the fate of reactive solutes at the stream scale. Numerical simulations show that whole-stream transformation is 5-25× greater when HZ reaction rates are highest near the SWI, compared to a stream with the same average reactivity uniformly distributed in the HZ (Li et al., 2017). These differences arise because solutes entering the HZ typically propagate through shallow, high reactivity flowpaths before returning to the water column. Process-based models must therefore account for the correlation between residence time in the stream and residence time in reactive regions of the river bed. Traveltime based approaches for advection-dominated hyporheic flows account for the variability of reaction rates between flow paths by assuming that fluid parcels move unmixed through the HZ (Azizian et al., 2015; Reeder et al., 2018). However, we currently lack a physics-based upscaling framework that accounts for the joint impact of spatially varying reaction rates and diffusive mass transfer in the HZ. This knowledge gap limits our understanding of how measurable features of the HZ contribute to river corridor biogeochemistry, as well as how long streamborne contaminants are retained in the benthic biolayer and the less reactive sublayer that can act as a secondary source.

This work is motivated by the questions of how the size and reactivity of the benthic biolayer influence reach-scale mass fate, and how these properties manifest in upscaled observations of reactive transport. We isolate the effects of depth-dependent HZ reaction rates on upscaled predictions of solute fate in a stream. Solute transport in the HZ is considered to be dominated by vertical diffusion, which aligns our analysis with existing diffusion-based scaling laws that predict hyporheic exchange fluxes from measurable stream parameters. We present streambed-scale and reach-scale simulations designed to mimic a pulse tracer injection, which is a common method for assessing the processes controlling reactive transport in rivers and whose results are extendable to other boundary conditions (e.g., plateau injection experiments). We compare numerical results to predictions from a classical mobile-immobile model with uniform reactions in the subsurface, as well as predictions from a novel mobile-immobile model that explicitly represents the vertically-varying reaction profile in the biolayer.

2 Methods

2.1 Transport scenario

We consider the transport and reaction scenario illustrated in Figure 1 that comprises the water column and HZ. The SWI is located at $z = 0$, the water column extends from $z = 0$ to $z = d$, and the HZ extends from $z = -h$ to $z = 0$. We set the stream velocity to $v(z) = v_s + v_0\kappa^{-1}\ln(z/z_0)$ for $z > z_0$ and zero for $z < z_0$ (Fischer et al., 1979). The length z_0 is the width of a roughness layer at the SWI and represents the effect of the porous streambed on the stream velocity, $\kappa \approx 0.41$ is the von Karman coefficient, v_0 the shear velocity, and v_s the slip velocity at the SWI. We set $v(z) = 0$ in the HZ, which assumes that streamwise velocity in the HZ is negligible compared to the stream. Vertical mixing is quantified by the dispersion coefficient $D(z)$, which is set equal to $D(z) = \kappa v_0 z(1 - z/d)$ for $z > z_0$ in the water column (Fischer et al., 1979) and equal to the constant effective diffusivity D_h in the HZ (Grant et al., 2012). We disregard streamwise dispersion and diffusion because advection in the water column dominates streamwise transport.

Solutes undergo first-order reactions in the HZ, which is a reasonable assumption when the modeled solute is limiting, that is, reactions are independent of the concen-

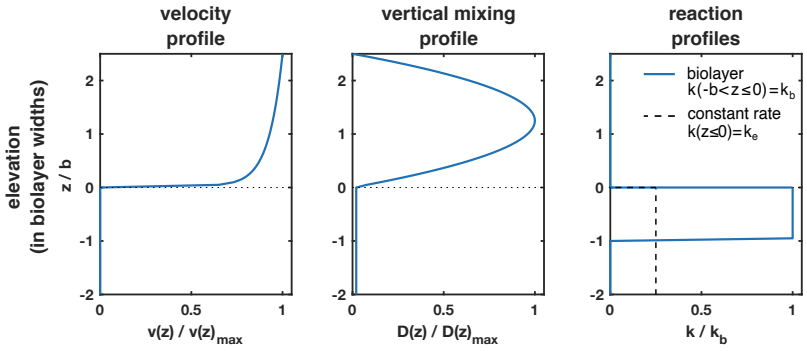

Figure 1. (Left to right) Spatial velocity, vertical mixing, and reaction profiles across the surface-subsurface continuum. The SWI is located at $z = 0$. The figures are truncated at $z/b = -2$ since all values are constant at deeper locations in the HZ.

tration of co-reactants, abundance of catalysts such as enzymes, or thermodynamic constraints (Dodds et al., 2002; Garayburu-Caruso et al., 2020). The depth-dependent reaction rate $k(z)$ can be an arbitrary function of streambed elevation, but typically decreases sharply with depth due to the presence of a reactive biolayer. We follow Li et al. (2017) and consider a biolayer structure consistent with field observations (Knapp et al., 2017; Schaper et al., 2019; Inwood et al., 2007; O'Connor & Harvey, 2008). The reaction rate is set to $k(z) = k_b$ within a layer of thickness b just below the SWI. It is set to $k(z) = 0$ in the non-reactive sublayer of thickness $\ell = h - b$. Other profiles that decay on a characteristic length scale b are expected to show a qualitatively similar behavior. The characteristic time scales in the HZ are given by the characteristic reaction time $\tau_r = k_b^{-1}$, as well as the characteristic diffusion times $\tau_h = h^2/D_h$ across the HZ, $\tau_b = b^2/D_h$ across the biolayer, and $\tau_\ell = \ell^2/D_h$ across the non-reactive sublayer. The Damköhler number $Da = \tau_b k_b$ compares the diffusion and reaction times in the biolayer. We consider the order of time scales $\tau_r \leq \tau_b < \tau_\ell$, which means that $Da \geq 1$. This implies that reactions can occur before solute is transmitted to the sublayer. If, on the contrary $\tau_r > \tau_b$ (i.e., $Da < 1$), only a small amount of solute can react before it reaches the sublayer. In this case, the behaviors of reactive and conservative solutes are very similar, and thus are not presented. The evolution of solute concentration $C(x, z, t)$ in the combined stream-HZ system is expressed by the advection-dispersion equation

$$\theta(z)\frac{\partial C}{\partial t} + v(z)\frac{\partial C}{\partial x} - \frac{\partial}{\partial z}\left[\theta(z)D(z)\frac{\partial C}{\partial z}\right] = -\theta(z)k(z)C, \tag{1}$$

where the porosity $\theta(z)$ equals 1 in the water column and a constant value θ_h in the HZ. The horizontal boundaries $z = -h$ and $z = d$ are impermeable. In line with the experimental design of field tracer studies, we assume that the HZ is initially free of reactive mass, and solute is introduced as a line injection in the water column. The direct advection-dispersion problem (1) is solved numerically using a reactive time-domain random walk approach (TDRW), based on the implementation of Russian et al. (2016) for conservative solutes. The TDRW method is computationally efficient for media with spatially heterogeneous advection, diffusion and reaction properties. Details on the implementation, discretization, and parameterization of the TDRW simulations are given in supporting information Section SI-VI. In the following, we present the mobile-immobile model that upscales this reactive transport scenario. In order to analyze the impact of the benthic biolayer on whole stream reactive transport, we consider solute breakthrough curves at a downstream control plane for different biolayer scenarios.

2.2 Mobile-immobile biolayer (MIM-B) model

We employ a mobile-immobile approach (Villermaux, 1974; Haggerty & Gorelick, 1995) to upscale the reactive transport problem. Eq. (1) is decomposed into an advection-dispersion equation for transport in the stream, a diffusion-reaction equation for the biolayer, and an equation for vertical diffusion in the sublayer. These equations are coupled through concentration and flux continuity at their respective interfaces. By vertical averaging we obtain a temporally non-local evolution equation for the average stream concentration $\overline{C}_s(x,t)$:

$$\frac{\partial}{\partial t}\overline{C}_s + \frac{\theta_h}{d}\frac{\partial}{\partial t}\int_0^t dt' \varphi_h(t-t')\overline{C}_s(x,t') + \overline{v}\frac{\partial \overline{C}_s}{\partial x} - D^*\frac{\partial^2 \overline{C}_s}{\partial x^2} = -\frac{\theta_h k_b}{d}\int_0^t dt' \varphi_b(t-t')\overline{C}_s(x,t'). \tag{2}$$

Details are provided in Section SI-II of the supporting information. The mean velocity in the stream is denoted by $\overline{v}$, and the shear dispersion coefficient $D^* = 5.93 v_0 d$ (Fischer et al., 1979) quantifies the impact of vertical velocity variability on longitudinal dispersion in the stream. The non-local term (second term on left side) denotes the time derivative of the concentration in the HZ. It quantifies solute trapping, release, and degradation in the hyporheic zone. The term on the right side demonstrates that the upscaled reaction kinetics are temporally non-local, but nonetheless linear. The non-locality stems from the fact that solute first diffuses into the biolayer before it reacts. Thus, the mass degraded at a given time t is proportional to the stream concentrations $\overline{C}_s(x,t')$ at earlier times t'. The memory kernel $\varphi_h(t)$ describes the evolution of mass in the HZ in response to an instantaneous solute pulse at the SWI. It is decomposed into $\varphi_h(t) = \varphi_b(t) + \varphi_0(t)$, wherein $\varphi_b(t)$ and $\varphi_0(t)$ encode the diffusive and reactive mass transfer mechanisms across the biolayer and the non-reactive sublayer, respectively. Explicit Laplace space expressions for $\varphi_b(t)$ and $\varphi_0(t)$ are given in Section SI-II C. While this formulation can be generalized to account for water column reactions (sensu Roche et al., 2019), we exclusively model reactions in the HZ to elucidate the biolayer's influence on stream-scale reactivity.

2.3 Surrogate models

To illustrate the benthic biolayer's impact on whole stream reactive transport, we contrast the MIM-B with two surrogate models, termed *S1* and *S2*. Model *S1* assumes the hyporheic zone is uniformly reactive over all depths. Model *S2* assumes that water column and HZ are in equilibrium.

2.3.1 Fully reactive hyporheic zone (S1)

In agreement with classical assumptions (e.g., Runkel, 2007; Haggerty et al., 2009; Aubeneau et al., 2015), *S1* assumes that the HZ is fully reactive and characterized by an equivalent reaction rate k_e. The evolution equation for $\overline{C}_s$ is obtained from (2) by substituting k_b with k_e and setting $\varphi_h(t) = \varphi_b(t) \equiv \varphi_e(t)$. The latter can be written in terms of the memory kernel $\phi(t)$ for a non-reactive solute as $\varphi_e(t) = \phi(t)\exp(-k_e t)$ (Dentz et al., 2011). We define k_e such that the total reacted mass in the HZ, in response to an instantaneous solute pulse at the SWI, is equal to the total reacted mass in the MIM-B. Using this definition, we derive the following transcendental equation for k_e (see, SI-IV)

$$\sqrt{\frac{k_e}{k_b}}\tanh\left(\sqrt{k_e \tau_h}\right) = \tanh\left(\sqrt{Da}\right). \tag{3}$$

The solution of (3) can be approximated by $k_e = k_b \tanh\left(\sqrt{Da}\right)^2$ for $k_e\tau_h > 10$. This implies that the equivalent streambed reactivity increases monotonically with Da and asymptotes towards k_b as $Da \to \infty$.

2.3.2 Equilibrium model for the water column (S2)

Model *S2* assumes that the water column and the HZ are in equilibrium. The evolution equation for $\overline{C}_s$ in this limit is obtained from Eq. (2) by localization of the memory kernels on the left and right sides. This gives (Section SI-V)

$$R_a \frac{\partial}{\partial t}\overline{C}_s + \overline{v}\frac{\partial \overline{C}_s}{\partial x} - D^* \frac{\partial^2 \overline{C}_s}{\partial x^2} = -k_a \overline{C}_s(x,t'), \tag{4}$$

where the apparent retardation coefficient R_a and the apparent reaction rate k_a are defined by

$$R_a = 1 + \frac{\theta_h}{d}\int_0^\infty dt' \varphi_h(t'), \qquad k_a = \frac{\theta_h k_b}{d}\int_0^\infty dt' \varphi_b(t'). \tag{5}$$

2.4 Reach-scale reactivity

The two surrogate models *S1* and *S2* are defined such that they have the same downstream mass recovery as the MIM-B model. The fraction of mass recovered M_R at a downstream location is obtained by integration of the solute breakthrough curves over time from zero to infinity. Thus, we obtain from *S2* the explicit expression

$$M_R(x) = \exp\left[-\frac{x\overline{v}}{2D^*}\left(\sqrt{1+\frac{4k_a D^*}{\overline{v}^2}} - 1\right)\right]. \tag{6}$$

This predicted exponential decrease is commonly observed in field experiments. The reach scale reactivity K_r [L^{-1}] has been defined in the literature as the slope of the logarithm of $M_R(x)$, that is, $K_r \equiv -x^{-1}\ln M_R(x)$ (Tank et al., 2017). Reach scale reactivity K_r reads in terms of the apparent reaction rate k_a as

$$K_r = \frac{\overline{v}}{2D^*}\left(\sqrt{1+\frac{4k_a D^*}{\overline{v}^2}} - 1\right). \tag{7}$$

Eq. (7) simplifies to $K_r = k_a \overline{v}^{-1}$ in the limit $D^* \to 0$, meaning that M_r decays as $\exp(-\tau_a k_a)$ in this limit, where $\tau_a = x\overline{v}^{-1}$ is the advective travel time. Note that K_r is not a reaction rate. It facilitates the estimation of reach-scale mass removal integrated over all times. This is important to note because the time scales for reaction can be very large due to mass transfer limitation in the HZ, which has a dramatic impact on contaminant removal and secondary release as discussed below. The evaluation of K_r is one of several methods that are often inter-compared to determine reach-scale reaction kinetics (e.g., Finkler et al., 2021). For ease of interpretation, we present reach-scale reactivity as uptake velocities, which are commonly used for comparison across rivers. The inverse of K_r denotes the nutrient spiraling length $S_w = K_r^{-1}$ [L], which describes the characteristic distance a reactant travels downstream before reacting. The uptake velocity $v_f = K_r \overline{v} d$ [$\mathrm{L\,T^{-1}}$] measures demand for reactants relative to in-stream concentration (Tank et al., 2017).

3 Results and discussion

3.1 Interplay between biolayer structure and solute fate in the HZ

Memory functions, which quantify the mass in the HZ resulting from an instantaneous solute pulse at the SWI, are shown in Figure 2 for (a) the sublayer, (b) the bi-

olayer, and (c) the entire HZ, obtained from the direct numerical simulations and the analytical MIM-B.

The sublayer memory function φ_0 increases from 0 to a maximum on the time scale τ_b, which is the time for solute tansmission across the biolayer. It then decreases as $t^{-1/2}$, as for a conservative solute, due to diffusion back to the biolayer. Last, it tempers exponentially on the time scale τ_ℓ as the sublayer depletes by diffusion.

The memory function φ_b for the biolayer decays as $t^{-1/2}$ for times smaller than the reaction time, $t < \tau_R$, due to diffusion across the SWI. For $\tau_R < t < \tau_b$ mass is depleted from the biolayer by chemical reaction, which manifests in an exponential decrease of φ_b (Figure 2b). For times $t \gg \tau_b$, the biolayer can be considered well-mixed, and φ_b transitions to a $t^{-3/2}$ decay because mass in the biolayer changes in a quasi-static fashion due to the mass flux from the sublayer (see SI-II D),

$$\varphi_b(t) = -\frac{\tau_b}{1+Da}\frac{\mathrm{d}\varphi_0}{\mathrm{d}t} \propto t^{-3/2}. \tag{8}$$

The memory function φ_h integrates the diffusion-reaction process in the biolayer and retention in the sublayer (Figure 2c). For times $t \ll \tau_R$, mass removal in the streambed is primarily caused by diffusion upward across the SWI, and we observe the characteristic $t^{-1/2}$ decay of a conservative solute. As discussed above, solute is depleted by reaction in the biolayer for $\tau_R < t < \tau_b$, giving rise to an exponential decay of φ_h. For $t < \tau_b$ all remaining mass resides at shallow depth in the benthic biolayer, and the system behaves as a scenario of constant streambed reactivity. For $t > \tau_b$, however, solute diffuses into the inert sublayer. Eventually, most mass remaining in the streambed is sequestered below the biolayer. The upward diffusion of mass from the inert sublayer into the biolayer results in a second regime of $\varphi_h(t) \sim t^{-1/2}$ (Figure 2c) because diffusion from the sublayer through the biolayer and to the stream is the dominant depletion process. Exponential tempering of $\varphi_h(t)$ then occurs on the time scale τ_ℓ (Figure 2c). For comparison, we show memory functions for the corresponding surrogate model *S1* parameterized with k_e (Figure 2c dotted line). It decays as $t^{-1/2}$ for times smaller than the reaction time $\tau_e = k_e^{-1}$ and exponentially fast for $t > \tau_e$ as solute degrades throughout the HZ. Thus, *S1* predicts much faster depletion of reactant than the MIM-B because it does not account for long survival in the sublayer.

In summary, the interaction of reaction and diffusion processes in the HZ is governed by three distinct timescales: the characteristic reaction time $\tau_R = k_b^{-1}$, which sets the time for solute depletion from the biolayer by reaction; the diffusion time τ_b, which sets the time for solute transmission through the biolayer to the inert sublayer; and τ_ℓ, which sets the time for diffusive depletion of solute from the sublayer. The match between simulated and modeled memory functions shows that the MIM-B correctly captures the long survival times in the HZ and the spatial segregation of reactants between the biolayer and the non-reactive sublayer.

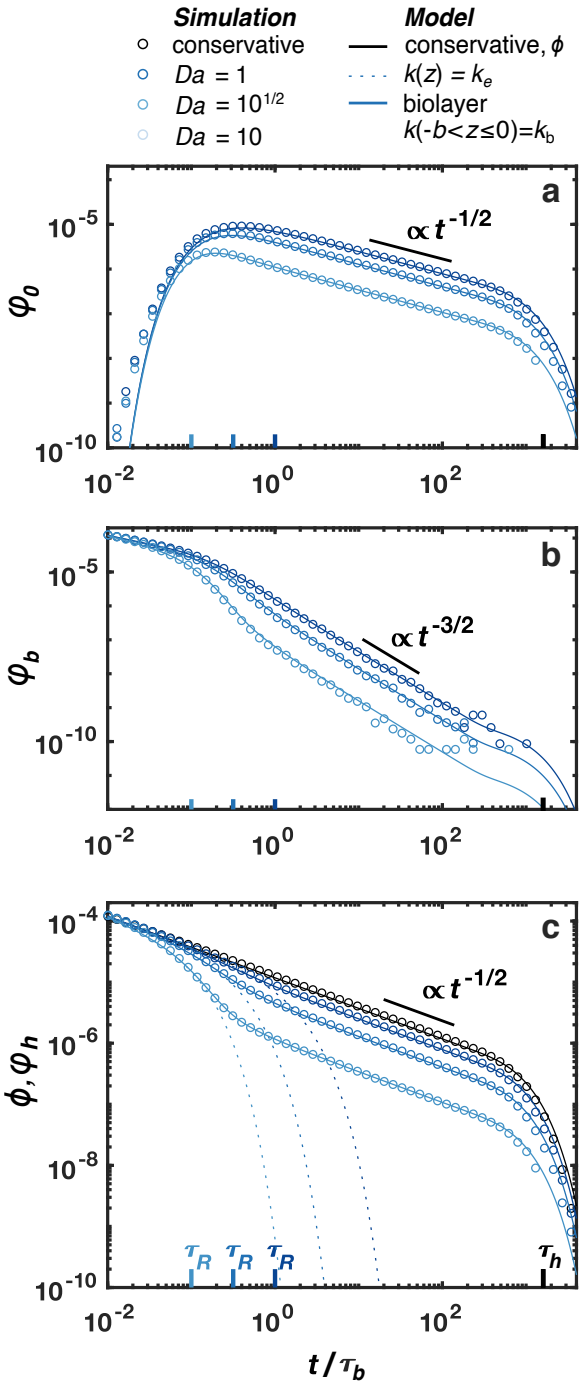

Figure 2. Modeled and simulated memory functions of varying biolayer Da. a) Memory functions for the inert sublayer show all mass in $-h \leq z < b$. b) Memory functions for the benthic biolayer show all mass in $-b \leq z < 0$. c) Full memory functions for conservative (black) and reactive (colored) solutes. Model and simulations transition to $t^{-1/2}$ tailing for $t \gg \tau_b(1+Da)^{-1}$. For all experiments, $b = 0.05\,\mathrm{m}$, $D_h = 1.042 \times 10^{-6}\,\mathrm{m^2 s^{-1}}$, $h = -2\,\mathrm{m}$, and k_b is varied.

3.2 Reach-scale observations and model predictions

3.2.1 Breakthrough curves

Figure 3 shows BTCs for conservative and reactive solutes from numerical simulations and MIM-B model predictions, as well as MIM-B prediction for the biolayer concentration at a control plane 100 m downstream from the injection point. These results are compared to the prediction of surrogate model *S1* for a fully reactive HZ. The conservative BTC decays as a power law with $t^{-3/2}$ and is cut off at the characteristic diffusion time across the HZ. This behavior is characteristic of diffusive mass transfer and secondary release from the HZ. The BTC for the reactive solute shows the same tailing features as the conservative BTC, albeit at lower concentrations due to degradation in the biolayer. The strong tailing of the contaminant concentration is caused by transmission of unreacted solute to the sublayer and release back into the stream through the biolayer. These behaviors are correctly quantified by the MIM-B, which predicts similar behavior for the contaminant concentration in the biolayer. This shows that both the stream and the biolayer are sourced by upward diffusion of solute sequestered in the sublayer. Results mirror results from memory function simulations, demonstrating that biolayer structure has a similar influence on degradation timescales at both the local scale and the whole-stream scale. On the other hand, *S1* predicts exponential decay of the BTC on the reaction timescale and thus severely under-predicts late time contaminant levels.

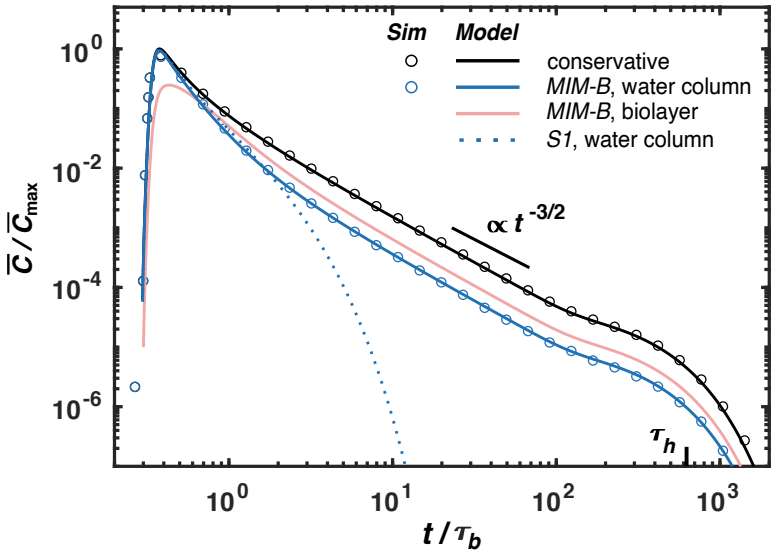

Figure 3. Simulated and MIM-B predicted BTCs for a pulse tracer injection with $x = 100$ m and $b = 0.08$ m, corresponding to $Da = 1.2$. See Section SI-VI for other parameter values. $C_{\max}$ equals maximum concentration of the analytical solution for the conservative BTC.

The exact match between simulated BTCs and MIM-B predictions demonstrates that the MIM-B fully captures the impact of long survival times in the HZ, as well as the spatial segregation of reactants in the HZ, on reach scale transport and degradation. Notably, the model predicts a power law decay of survival times for all Da. This indicates the potential of MIM-B to provide correct estimates of trace contaminants in benthic sediments and the stream over a range of different physical and chemical conditions in the HZ. Trace organic contaminants (TOCs) are now detected in most rivers (Bernhardt

et al., 2017) and impair stream ecosystems at low levels, for example, endocrine disrupting compounds that alter fish physiology at nanomolar concentrations (Adeel et al., 2017; Khanal et al., 2006). Degradation rates of TOCs decrease rapidly with depth in the HZ and span a range of half lives (Kunkel & Radke, 2008; Schaper et al., 2019). These characteristics allow TOCs to persist in sediments long after they enter the river network and act as a secondary source (Ciparis et al., 2012; Cozzarelli et al., 2017). This suggests that their degradation timescales must be estimated by explicitly accounting for the vertically varying reaction rates in the HZ (see SI-VII).

3.2.2 Reach-scale reactivity

Calculated v_f resulting from integration of the simulated BTC, sensu Tank et al. (2008), agrees well with the analytical prediction from the MIM-B model (Eq. 7, Figure 4). The plot also shows that v_f approaches an asymptotic value for values b larger than the characteristic survival depth $s = (D_h/k_b)^{1/2}$, which denotes the diffusion length during the reaction times τ_R. This implies that the spatial extension of the the biolayer has little bearing on whole-stream reactivity for $b > s$. When $b \gg s$, nearly all solute reacts before propagating below the biolayer. In contrast, a substantial amount of mass propagates through the biolayer unreacted when $b < s$, resulting in a lower effective reactivity of the HZ (see SI-VII) and a lower reach-scale reactivity.

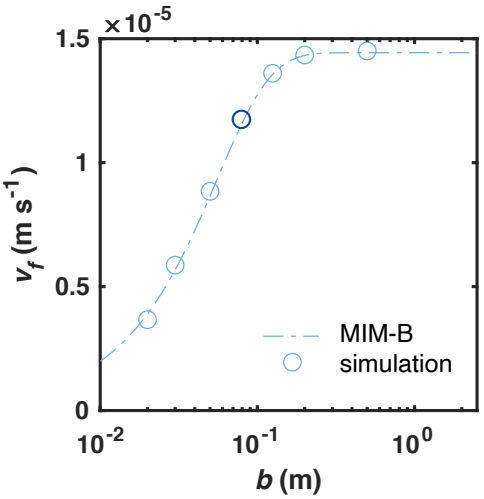

Figure 4. Reach-scale reactivity reported as uptake velocity, for streambeds containing biolayers with varying b. The reaction rate is $k_b = 2.0 \times 10^{-4}$ s^{-1} and corresponds to a characteristic survival depth of $s = 0.07$ m. See Section SI-VI for all parameter values. Dark blue circle is result from the simulation shown in Figure 3.

The MIM-B gives exact estimates of reach-scale reactivity under the assumed conditions of diffusion dominated transport and stratified reactivity in the HZ. It should be emphasized that these estimates are only valid when made at asymptotic times. Transient storage in the HZ delays transport through the reach, causing mass to arrive significantly later than the advective timescale $\tau_a = x\,\overline{v}^{-1}$, upon which metrics such as v_f are typically based. This delay can cause time-resolved methods for estimating reach-scale reactivity to deviate systematically from the reactivity calculated from integrated mass transformation. For example, results from pulse tracer injection experiments are commonly used to calculate a different effective reaction rate for each data point of the BTC, wherein the reaction time is set to the breakthrough time (Covino et al., 2010).

The effective rates calculated from this method depend nonlinearly on reactant concentration even when reactions within the reach are linear, which may lead to the conclusion that reaction kinetics are nonlinear (Li et al., 2021). Integrated methods, such as integration of the BTC or constant rate injection experiments, account for the transport and reaction delays associated with non-local transport to the HZ and mass sequestration below the biolayer. Nevertheless, using these methods may require very long observation times in order to account for the power law decay of reactive mass released from the sublayer, and they provide no information about when concentrations may exceed critical thresholds. Finally, it is important to note that neither method gives information on the actual reaction kinetics and time evolution of the downstream contaminant concentration. The derived upscaled MIM-B shows that reaction kinetics are in fact nonlocal as expressed by the right side of Eq. (2) and characterized by a power-law decay of contaminant survival times.

4 Conclusion

Two fundamental challenges for providing mechanistic predictions of river corridor reactivity are to explicitly link local heterogeneity of the controlling physical processes to upscaled observations within a consistent modeling framework, and to identify the relative importance of microscale processes and structural features of the river corridor (Ward & Packman, 2019; Kelleher et al., 2019). We address these challenges by analyzing and upscaling reactive transport in a river-streambed system characterized by a benthic biolayer. Isolating the dominant small scale features, we derive a novel upscaled model (MIM-B) that captures the dominant physical and chemical processes in the benthic biolayer, the HZ, and reach scale. The model predictions closely agree with detailed numerical simulations of transport and reaction in the river-streambed system.

We find that the biolayer structure strongly controls solute degradation in the HZ and at the reach scale. Accumulation in the sublayer leads to long survival times for reactive solute, characterized by a power-law decay of concentration and by the spatial segregation of mass in the HZ. This is in stark contrast to model predictions based on the classical assumption of a fully reactive HZ, for which the contaminant concentration decays exponentially fast on the characteristic reaction time scale and thus strongly underpredicts contaminant levels in the tail. The novel MIM-B captures all aspects of contaminant degradation on the HZ and reach scales. Specifically, it correctly predicts tail concentrations and reach scale reactivity. Reach scale reactivity quantifies the reaction potential of the system; however, this potential can in principle only be observed at very long experimental times due to the role of the sublayer as a secondary release.

Although we assume solutes diffuse vertically through the HZ in order to align our model with empirical scaling laws, we expect similar qualitative behavior in any streambed with vertically varying reaction rates and a multiscale residence time distribution (e.g., Elliott & Brooks, 1997). The characteristics of reactant fate identified within our model framework are critical for assessing contamination levels in streams and in shallow sediments, which are dramatically underestimated at late times by classical models that assume uniform reaction rates in the hyporheic zone.

Acknowledgments

KRR was supported by a junior scholar fellowship to Spain from the Fulbright Program. MD acknowledges the support of the Spanish Ministry of Science and Innovation (project HydroPore PID2019-106887GB-C31). Numerical data generated for this publication is based on the model of Russian et al. (2016), as described in the main text and supporting information. High-performance computing support of the R2 (DOI: 10.18122/B2S41H) and Borah (DOI: 10.18122/oit/3/boisestate) computer clusters was provided by Boise State Universitys Research Computing Department.

References

Abramowitz, M., & Stegun, I. A. (1964). *Handbook of mathematical functions with formulas, graphs, and mathematical tables* (Vol. 55). US Government printing office.

Adeel, M., Song, X., Wang, Y., Francis, D., & Yang, Y. (2017, February). Environmental impact of estrogens on human, animal and plant life: A critical review. *Environment International*, *99*, 107–119. Retrieved 2020-06-10, from http://www.sciencedirect.com/science/article/pii/S0160412016304494 doi: 10.1016/j.envint.2016.12.010

Aubeneau, A. F., Drummond, J. D., Schumer, R., Bolster, D., Tank, J. L., & Packman, A. I. (2015, March). Effects of benthic and hyporheic reactive transport on breakthrough curves. *Freshwater Science*, *34*(1), 301–315. Retrieved 2019-04-10, from https://www.journals.uchicago.edu/doi/10.1086/680037 doi: 10.1086/680037

Azizian, M., Grant, S. B., Kessler, A. J., Cook, P. L. M., Rippy, M. A., & Stewardson, M. J. (2015, September). Bedforms as Biocatalytic Filters: A Pumping and Streamline Segregation Model for Nitrate Removal in Permeable Sediments. *Environmental Science & Technology*, *49*(18), 10993–11002. Retrieved 2020-07-24, from https://doi.org/10.1021/acs.est.5b01941 doi: 10.1021/acs.est.5b01941

Battin, T. J., Kaplan, L. A., Findlay, S., Hopkinson, C. S., Marti, E., Packman, A. I., ... Sabater, F. (2008, February). Biophysical controls on organic carbon fluxes in fluvial networks. *Nature Geoscience*, *1*(2), 95–100. Retrieved 2019-04-10, from http://www.nature.com/articles/ngeo101 doi: 10.1038/ngeo101

Bernhardt, E. S., Rosi, E. J., & Gessner, M. O. (2017, March). Synthetic chemicals as agents of global change. *Frontiers in Ecology and the Environment*, *15*(2), 84–90. Retrieved 2020-07-28, from https://doi.org/10.1002/fee.1450 (Publisher: John Wiley & Sons, Ltd) doi: 10.1002/fee.1450

Cardenas, M. B., Ford, A. E., Kaufman, M. H., Kessler, A. J., & Cook, P. L. M. (2016, December). Hyporheic flow and dissolved oxygen distribution in fish nests: The effects of open channel velocity, permeability patterns, and groundwater upwelling. *Journal of Geophysical Research: Biogeosciences*, *121*(12), 3113–3130. Retrieved 2021-09-07, from https://onlinelibrary.wiley.com/doi/10.1002/2016JG003381 doi: 10.1002/2016JG003381

Carslaw, H., & Jaeger, J. (1959). Conduction of heat in solids. *Oxford: Clarendon Press*.

Ciparis, S., Iwanowicz, L. R., & Voshell, J. R. (2012, January). Effects of watershed densities of animal feeding operations on nutrient concentrations and estrogenic activity in agricultural streams. *Science of The Total Environment*, *414*, 268–276. Retrieved 2021-05-14, from https://www.sciencedirect.com/science/article/pii/S0048969711011764 doi: 10.1016/j.scitotenv.2011.10.017

Covino, T. P., McGlynn, B. L., & McNamara, R. A. (2010). Tracer Additions for Spiraling Curve Characterization (TASCC): Quantifying stream nutrient uptake kinetics from ambient to saturation. *Limnology and Oceanography: Methods*, *8*(9), 484–498. Retrieved from http://dx.doi.org/10.4319/lom.2010.8.484 doi: 10.4319/lom.2010.8.484

Cozzarelli, I. M., Skalak, K. J., Kent, D. B., Engle, M. A., Benthem, A., Mumford, A. C., ... Jolly, G. D. (2017, February). Environmental signatures and effects of an oil and gas wastewater spill in the Williston Basin, North Dakota. *Science of The Total Environment*, *579*, 1781–1793. Retrieved 2021-05-15, from https://www.sciencedirect.com/science/article/pii/S0048969716326201 doi: 10.1016/j.scitotenv.2016.11.157

Dentz, M., Gouze, P., Russian, A., Dweik, J., & Delay, F. (2012, December). Diffusion and trapping in heterogeneous media: An inhomogeneous continuous time

random walk approach. *Advances in Water Resources*, *49*, 13–22. Retrieved 2021-04-16, from https://www.sciencedirect.com/science/article/pii/S0309170812002035 doi: 10.1016/j.advwatres.2012.07.015

Dentz, M., Le Borgne, T., Englert, A., & Bijeljic, B. (2011, March). Mixing, spreading and reaction in heterogeneous media: A brief review. *Journal of Contaminant Hydrology*, *120-121*, 1–17. Retrieved 2019-04-10, from https://linkinghub.elsevier.com/retrieve/pii/S0169772210000495 doi: 10.1016/j.jconhyd.2010.05.002

Dodds, W. K., López, A. J., Bowden, W. B., Stan Gregory, Grimm, N. B., Hamilton, S. K., ... Wilfred Wollheim (2002). N uptake as a function of concentration in streams. *Journal of the North American Benthological Society*, *21*(2), 206–220. Retrieved from https://doi.org/10.2307/1468410 doi: 10.2307/1468410

Elliott, A. H., & Brooks, N. H. (1997, January). Transfer of nonsorbing solutes to a streambed with bed forms: Theory. *Water Resources Research*, *33*(1), 123–136. Retrieved 2019-04-10, from http://doi.wiley.com/10.1029/96WR02784 doi: 10.1029/96WR02784

Finkler, N. R., Gücker, B., Boëchat, I. G., Tromboni, F., Thomas, S. A., Mendes, L. A., ... others (2021). Comparing spiraling- and transport-based approaches to estimate in-stream nutrient uptake length from pulse additions. *Ecohydrology*, e2331.

Fischer, H. B., List, J. E., Koh, C. R., Imberger, J., & Brooks, N. H. (1979). *Mixing in inland and coastal waters*. Academic press.

Garayburu-Caruso, V. A., Stegen, J. C., Song, H.-S., Renteria, L., Wells, J., Garcia, W., ... Graham, E. B. (2020, May). Carbon Limitation Leads to Thermodynamic Regulation of Aerobic Metabolism. *Environmental Science & Technology Letters*. Retrieved 2020-06-12, from https://doi.org/10.1021/acs.estlett.0c00258 doi: 10.1021/acs.estlett.0c00258

Grant, S. B., Stewardson, M. J., & Marusic, I. (2012, May). Effective diffusivity and mass flux across the sediment-water interface in streams: EFFECTIVE DIFFUSION COEFFICIENT FOR HYPORHEIC EXCHANGE. *Water Resources Research*, *48*(5). Retrieved 2019-04-10, from http://doi.wiley.com/10.1029/2011WR011148 doi: 10.1029/2011WR011148

Haggerty, R., & Gorelick, S. M. (1995). Multiple-rate mass transfer for modeling diffusion and surface reactions in media with pore-scale heterogeneity. *Water Resources Research*, *31*(10), 2383–2400. (Publisher: Wiley Online Library)

Haggerty, R., Mart, E., Argerich, A., von Schiller, D., & Grimm, N. B. (2009, September). Resazurin as a smart tracer for quantifying metabolically active transient storage in stream ecosystems. *Journal of Geophysical Research*, *114*(G3), G03014. Retrieved 2019-04-10, from http://doi.wiley.com/10.1029/2008JG000942 doi: 10.1029/2008JG000942

Harvey, J. W., Bhlke, J. K., Voytek, M. A., Scott, D., & Tobias, C. R. (2013, October). Hyporheic zone denitrification: Controls on effective reaction depth and contribution to whole-stream mass balance: Scaling hyporheic flow controls on stream denitrification. *Water Resources Research*, *49*(10), 6298–6316. Retrieved 2019-04-10, from http://doi.wiley.com/10.1002/wrcr.20492 doi: 10.1002/wrcr.20492

Inwood, S. E., Tank, J. L., & Bernot, M. J. (2007, February). Factors Controlling Sediment Denitrification in Midwestern Streams of Varying Land Use. *Microbial Ecology*, *53*(2), 247–258. Retrieved from https://doi.org/10.1007/s00248-006-9104-2 doi: 10.1007/s00248-006-9104-2

Jones, J. B., & Mulholland, P. J. (1999). *Streams and Ground Waters*. Academic Press.

Kelleher, C., Ward, A., Knapp, J. L. A., Blaen, P. J., Kurz, M. J., Drummond, J. D., ... Krause, S. (2019). Exploring Tracer Informa-

tion and Model Framework Trade-Offs to Improve Estimation of Stream Transient Storage Processes. *Water Resources Research*, *55*(4), 3481–3501. Retrieved 2020-12-22, from https://agupubs.onlinelibrary.wiley.com/doi/abs/10.1029/2018WR023585 (_eprint: https://agupubs.onlinelibrary.wiley.com/doi/pdf/10.1029/2018WR023585) doi: https://doi.org/10.1029/2018WR023585

Khanal, S. K., Xie, B., Thompson, M. L., Sung, S., Ong, S.-K., & van Leeuwen, J. H. (2006, November). Fate, Transport, and Biodegradation of Natural Estrogens in the Environment and Engineered Systems. *Environmental Science & Technology*, *40*(21), 6537–6546. Retrieved 2020-06-10, from https://doi.org/10.1021/es0607739 (Publisher: American Chemical Society) doi: 10.1021/es0607739

Knapp, J. L. A., González-Pinzón, R., Drummond, J. D., Larsen, L. G., Cirpka, O. A., & Harvey, J. W. (2017, February). Tracer-based characterization of hyporheic exchange and benthic biolayers in streams: HYPORHEIC EXCHANGE AND BENTHIC BIOLAYERS. *Water Resources Research*, *53*(2), 1575–1594. Retrieved 2019-04-10, from http://doi.wiley.com/10.1002/2016WR019393 doi: 10.1002/2016WR019393

Kunkel, U., & Radke, M. (2008, October). Biodegradation of Acidic Pharmaceuticals in Bed Sediments: Insight from a Laboratory Experiment. *Environmental Science & Technology*, *42*(19), 7273–7279. Retrieved 2021-09-07, from https://pubs.acs.org/doi/10.1021/es801562j doi: 10.1021/es801562j

Li, A., Aubeneau, A. F., Bolster, D., Tank, J. L., & Packman, A. I. (2017, August). Covariation in patterns of turbulence-driven hyporheic flow and denitrification enhances reach-scale nitrogen removal: HYPORHEIC FLOW-DENITRIFICATION UPSCALING. *Water Resources Research*, *53*(8), 6927–6944. Retrieved 2019-04-10, from http://doi.wiley.com/10.1002/2016WR019949 doi: 10.1002/2016WR019949

Li, A., Bernal, S., Kohler, B., Thomas, S. A., Mart, E., & Packman, A. I. (2021). Residence Time in Hyporheic Bioactive Layers Explains Nitrate Uptake in Streams. *Water Resources Research*, *57*(2), e2020WR027646. Retrieved 2021-06-18, from https://agupubs.onlinelibrary.wiley.com/doi/abs/10.1029/2020WR027646 (_eprint: https://agupubs.onlinelibrary.wiley.com/doi/pdf/10.1029/2020WR027646) doi: 10.1029/2020WR027646

Marzadri, A., Dee, M. M., Tonina, D., Bellin, A., & Tank, J. L. (2017, April). Role of surface and subsurface processes in scaling N2O emissions along riverine networks. *Proceedings of the National Academy of Sciences*, *114*(17), 4330–4335. Retrieved 2021-02-15, from https://www.pnas.org/content/114/17/4330 doi: 10.1073/pnas.1617454114

Moran, P. W., Nowell, L. H., Kemble, N. E., Mahler, B. J., Waite, I. R., & Van Metre, P. C. (2017, December). Influence of sediment chemistry and sediment toxicity on macroinvertebrate communities across 99 wadable streams of the Midwestern USA. *Science of The Total Environment*, *599-600*, 1469–1478. Retrieved 2021-09-07, from https://linkinghub.elsevier.com/retrieve/pii/S004896971731135X doi: 10.1016/j.scitotenv.2017.05.035

O'Connor, B. L., & Harvey, J. W. (2008, December). Scaling hyporheic exchange and its influence on biogeochemical reactions in aquatic ecosystems: HYPORHEIC FLOW AND BIOGEOCHEMICAL REACTIONS. *Water Resources Research*, *44*(12). Retrieved 2019-04-10, from http://doi.wiley.com/10.1029/2008WR007160 doi: 10.1029/2008WR007160

Reeder, W. J., Quick, A. M., Farrell, T. B., Benner, S. G., Feris, K. P., Marzadri, A., & Tonina, D. (2018). Hyporheic Source and Sink of Nitrous Oxide. *Water Resources Research*, *54*(7), 5001–5016. Retrieved 2020-12-22, from https://agupubs.onlinelibrary

.wiley.com/doi/abs/10.1029/2018WR022564 (_eprint: https://agupubs.onlinelibrary.wiley.com/doi/pdf/10.1029/2018WR022564) doi: https://doi.org/10.1029/2018WR022564

Roche, K. R., Shogren, A. J., Aubeneau, A., Tank, J. L., & Bolster, D. (2019, February). Modeling Benthic Versus Hyporheic Nutrient Uptake in Unshaded Streams With Varying Substrates. *Journal of Geophysical Research: Biogeosciences*, *124*(2), 367–383. Retrieved 2019-04-10, from http://doi.wiley.com/10.1029/2018JG004684 doi: 10.1029/2018JG004684

Runkel, R. L. (2007). Toward a transport-based analysis of nutrient spiraling and uptake in streams. *Limnology and Oceanography: Methods*, *5*(1), 50–62.

Russian, A., Dentz, M., & Gouze, P. (2016). Time domain random walks for hydrodynamic transport in heterogeneous media. *Water Resources Research*, *52*(5), 3309–3323. (Publisher: Wiley Online Library)

Schaper, J. L., Posselt, M., Bouchez, C., Jaeger, A., Nuetzmann, G., Putschew, A., ... Lewandowski, J. (2019, April). Fate of Trace Organic Compounds in the Hyporheic Zone: Influence of Retardation, the Benthic Biolayer, and Organic Carbon. *Environmental Science & Technology*, *53*(8), 4224–4234. Retrieved 2021-01-19, from https://pubs.acs.org/doi/10.1021/acs.est.8b06231 doi: 10.1021/acs.est.8b06231

Tank, J. L., Reisinger, A. J., & Rosi, E. J. (2017). Nutrient Limitation and Uptake. In *Methods in Stream Ecology* (pp. 147–171). Elsevier. Retrieved 2019-04-10, from https://linkinghub.elsevier.com/retrieve/pii/B9780128130476000097 doi: 10.1016/B978-0-12-813047-6.00009-7

Tank, J. L., Rosi-Marshall, E. J., Baker, M. A., & Hall, R. O. (2008, October). Are rivers just big streams? A pulse method to quantify nitrogen demand in a large river. *Ecology*, *89*(10), 2935–2945. Retrieved 2019-04-10, from http://doi.wiley.com/10.1890/07-1315.1 doi: 10.1890/07-1315.1

Villermaux, J. (1974, December). Deformation of Chromatographic Peaks Under the Influence of Mass Transfer Phenomena. *Journal of Chromatographic Science*, *12*(12), 822–831. Retrieved 2019-04-10, from https://academic.oup.com/chromsci/article-lookup/doi/10.1093/chromsci/12.12.822 doi: 10.1093/chromsci/12.12.822

Ward, A. S., & Packman, A. I. (2019). Advancing our predictive understanding of river corridor exchange. *WIREs Water*, *6*(1), e1327. Retrieved 2020-12-22, from https://onlinelibrary.wiley.com/doi/abs/10.1002/wat2.1327 (_eprint: https://onlinelibrary.wiley.com/doi/pdf/10.1002/wat2.1327) doi: https://doi.org/10.1002/wat2.1327